

A comparison between Pa α and H α emission: the relation between mean H II region reddening, local gas density and metallicity¹

Alice C. Quillen & Mihoko Yukita

Steward Observatory, The University of Arizona, Tucson, AZ 85721; aquillen@as.arizona.edu

ABSTRACT

We measure reddenings to H II regions in NGC 2903, NGC 1512, M51, NGC 4449 and NGC 6946 from Hubble Space Telescope Pa α and H α images. Extinctions range from $A_V \sim 5 - 0$ depending upon the galaxy. For the galaxies with HST images in both lines, NGC 2903, NGC 1512 and M51, the Pa α and H α emission are almost identical in morphology which implies that little emission from bright H II regions is hidden from view by regions of comparatively high extinction. The scatter in the measured extinctions in each galaxy is only ± 0.5 mag.

We compare the reddenings we measure in five galaxies using the Pa α to H α ratios to those measured previously from the Balmer decrement in the LMC and as a function of radius in M101 and M51. We find that luminosity weighted mean extinctions of these ensembles of H II regions are correlated with gas surface density and metallicity. The correlation is consistent with the mean extinction depending on dust density where the dust to gas mass ratio scales with the metallicity. This trend is expected if H II regions tend to be located near the mid-plane of a gas disk and emerge from their parent molecular clouds soon after birth. In environments with gas densities below a few hundred M_\odot/pc^2 , star formation rates estimated from integrated line fluxes and mean extinctions are likely to be fairly accurate.

Subject headings:

1. Introduction

It has long been suspected that H II regions tend to exhibit higher reddenings in higher metallicity environments. For example, in M101 and M51 (Scowen, Dufour, & Hester 1992; Kennicutt & Garnett 1996; Scowen 1992) a trend between H II region extinction and galactic radius was observed and interpreted to be caused by the radial metallicity gradient in these galaxies. However, most studies have found a large scatter between the extinction and metallicity

¹Based on observations with the NASA/ESA *Hubble Space Telescope* obtained at the Space Telescope Science Institute which is operated by the Association of University for Research in Astronomy, Inc. (AURA), under NASA contract NAS5-26555.

in individual H II regions (McCall, Rybski & Shields 1985; Zaritsky, Kennicutt & Huchra 1994; Scowen et al. 1992; Kennicutt & Garnett 1996; Bresolin et al. 1999). Even though the metallicity is fairly uniform across the Large Magellanic Cloud (LMC), high values of the Balmer decrement are measured near 30 Doradus (Heydari-Mayaleri & Testor 1985; Caplan & Deharveng 1985) which is located in a region of high gas density (Cohen et al. 1988; Luks & Rohlfs 1992). Scowen et al. 1992 discovered a few H II regions in M101 with anomalously high extinctions at large galactic radii, which they attributed to higher local gas densities in nearby spiral arms. Despite the large scatter intrinsic to ensembles of H II regions, previous studies have found that the mean extinction of ensembles of H II regions varied between different galaxy regions. Martin & Friedli 1999 attributed the higher mean extinctions in H II regions in barred galaxies compared to non-barred galaxies to be caused by the higher gas densities associated with bar induced shocks. Scowen et al. 1992 and Scowen 1992 found that mean H II region redennings were higher at large galactic radii than at smaller radii in both M101 and M51.

If there is a general trend for an ensemble of H II regions to be more highly reddened in higher gas density or metal rich environments, then the star formation rate estimated from a sum of recombination line (such as $H\alpha$; e.g., Kennicutt 1998) fluxes would be underestimated in these environments. One way to quantify this effect is to measure extinctions towards ensembles of H II regions in a variety of different galactic environments. If mean H II region extinctions depend upon gas density and metallicity then it might be possible to formulate an empirical correction for the flux. This would allow star formation rates to be measured from one recombination line in more heavily reddened regions. If such a trend exists, star formation rates could be more accurately estimated for galaxies at high redshift and observed line ratios would also yield constraints on the galaxy metallicity and gas surface density.

By observing in the the near-infrared it is possible to probe into more heavily obscured regions because the near-infrared is less affected by dust extinction than optical wavelengths (for examples of previous work on infrared recombination lines see Calzetti et al. 1996 and Beck, Beckwith, & Gately 1984). The hydrogen $Pa\alpha$ recombination line at $1.875\mu\text{m}$ is bright in the vicinity of hot newly formed stars. It is difficult to observe in nearby galaxies from the ground because of strong atmospheric absorption from water molecules. It is expected to be about one eighth as bright as $H\alpha$ at temperatures and densities typical of H II regions, but since it is three times the wavelength of $H\alpha$ it should be less affected by extinction. For an H II region seen through a moderate foreground dust screen with $A_V \sim 3$, $Pa\alpha$ should be as bright as $H\alpha$. Previous studies of $Pa\alpha$ imaging in galaxies include Böker et al. 1999 and Marconi et al. 2000.

In this paper we measure $H\alpha$ and $Pa\alpha$ fluxes for H II regions in the central regions of five galaxies. We find that the scatter in A_V in each galaxy region is less than the differences in the mean values. Observations of distant galaxies are restricted towards observing line emission over a large region in the galaxy. Because of this we estimate a correction for the $H\alpha$ flux which is based upon summing over the extinction corrected fluxes of individual H II regions. This procedure is one way of averaging over the scatter in extinctions which has been observed in previous studies

of H II regions. We then investigate the dependence of this mean extinction on local gas density and metallicity.

2. Observations

We searched the HST archive for galaxies which have high quality narrow band images in Pa α and reveal a number of H II regions. The archived images are listed with their filters in Table 1. NGC 2903 and NGC 1512 have narrow band images taken by HST in both Pa α and H α , revealing a large number of H II regions. M51 also has both Pa α and H α images observed by HST showing numerous H II regions; however, these images overlap only in a small region about 20'' to the north and 20'' to the east of the nucleus. NGC 4449 and NGC 6946 have high quality Pa α images containing numerous H II regions but lack HST narrow band imaging in H α . For comparison we used H α fluxes for NGC 4449 measured by Scowen 1992 and a calibrated ground-based H α image for NGC 6946 provided by Rob Kennicutt (private communication). NGC 2903, NGC 4449 and NGC 6946 were observed as part of the nearby galaxies snap shot survey (Böker et al. 1999).

The NICMOS images were reduced with the *nicred* data reduction software (McLeod 1997) using on orbit darks and flats. The narrow band images required a pedestal correction which we assumed was an additional constant in each quadrant of the chip (for more discussion on this see Böker et al. 1999). WFPC2 images were combined using the IRAF/STSDAS routine *combine* which removed most of the cosmic ray hits. We derived H α and Pa α line emission images by subtracting scaled continuum images from the narrow band images containing the lines.

WFPC2 images were calibrated using zeropoints listed in the HST Data Handbook. Specifically we used 3.062×10^{-15} and 2.941×10^{-15} erg cm $^{-2}$ s $^{-1}$ /(DN s $^{-1}$) for the continuum subtracted F656N and F658N narrow band images, respectively in the PC camera of WFPC2. The NICMOS continuum subtracted narrow band images in the F187N filter were calibrated using 6.69×10^{-16} and 8.27×10^{-16} erg cm $^{-2}$ s $^{-1}$ /(DN s $^{-1}$) for Camera 2 and Camera 3 respectively for the Pa α line. The NICMOS broad-band images in the F160W filter were calibrated using 2.190×10^{-6} and 2.776×10^{-6} Jy/(DN s $^{-1}$) for Camera 2 and Camera 3 respectively. The NICMOS flux calibration is 10.7% lower than that used by Böker et al. 1999 and is based on measurements of the standard stars P330-E and P172-D during the Servicing Mission Observatory Verification program and subsequent observations (M. Rieke 1999, private communication). The filter widths listed in the NICMOS and WFPC2 instrument handbooks were used to derive the calibration corrections. The location of the lines was near the region of maximum transmission in the filters in all cases so no correction for filter transmission is required.

To measure the flux of emission regions we used aperture photometry. We identify individual regions from peaks in the Pa α line emission images. Aperture sizes were chosen to match the resolution of the H α images or that of existing H α photometry (for NGC 4449 to match that of Scowen 1992). For NGC 2903, NGC 1512, and M 51, because we had HST imaging in both

lines we were able to use very small apertures. In all cases identical aperture positions and sizes were used on both line emission images. Fluxes and identified regions are listed in Tables 2-6. Positions are given with respect to the nucleus as defined by the centroid at the brightest spot in the NICMOS/F160W images. The positions of nuclei are listed in Table 2-6. Astrometry was done with the IRAF/STSDAS routine *xy2rd* from the F160W images and is that determined by the HST pointing.

We use the $\text{H}\alpha/\text{Pa}\alpha$ line ratios to estimate the extinction to each region. We assume intrinsic flux ratios of $F_{\text{H}\alpha}/F_{\text{H}\beta} = 2.86$, $F_{\text{H}\alpha}/F_{\text{Pa}\alpha} = 8.46$ for Case B recombination at a temperature of 10^4K and a density 100 cm^{-3} (line ratios are given in Osterbrock 1989) and a Galactic extinction law (Mathis 1990). For NGC 2903 and M51 the $[\text{NII}]6584\text{\AA}$ line was not contained in the F656N filter, however it is contained in the F658N image of NGC 1512. We correct for the presence of this line in NGC 1512 and NGC 6946 assuming a $\text{H}\alpha/(\text{H}\alpha + [\text{NII}])$ line ratio of 0.75 (following the procedure of Kennicutt 1983). We corrected for Galactic redenning using values from Schlegel et al. 1998.

Fluxes and extinctions derived from $\text{Pa}\alpha/\text{H}\alpha$ flux ratios are listed in Tables 2-6. The variations in the intrinsic line ratios caused by temperature differences are unlikely to significantly affect the measured extinctions; (lowering the electron temperature by 5000K results in a reduction of 15% in the $\text{H}\alpha/\text{Pa}\alpha$ line ratio). The errors in the measured line ratios are dominated by errors in the sky value caused by color variations which affect our continuum subtraction or the uneven sky in the $\text{Pa}\alpha$ images caused by the pedestal affect. The photometric uncertainties are roughly estimated in the Table captions. There is an additional error in the absolute calibration of $\sim \pm 20\%$ which corresponds to an error of $\sim \pm 0.2$ in the derived A_V . Relative photometric error between individual H II regions in a galaxy are $\sim \pm 0.1$ mag in A_V for the faintest regions. The scatter, $\sim \pm 0.5$, in A_V in each galaxy is therefore likely to be intrinsic and not caused by photometric uncertainty.

When possible, we have compared our measured extinction values with those reported in previous studies. Two of the H II regions in NGC 6946 were also studied by Hyman et al. 2000 with radio continuum and $\text{H}\alpha$ observations. For the 3rd and 4th H II region listed in Table 5 we find $A_V \sim 3.2$, while Hyman et al. 2000 report $A_V \sim 2.5$ and 3.4, in rough agreement with our estimates.

Although Scowen 1992 measured a high extinction, $A_V \sim 2$, for many regions in NGC 4449 from his $\text{H}\alpha$ and $\text{H}\beta$ narrow band imaging, the $\text{Pa}\alpha/\text{H}\alpha$ line ratios that we compute from our $\text{Pa}\alpha$ photometry and his $\text{H}\alpha$ fluxes suggest that there is little internal extinction in this galaxy. However, our line ratios are consistent with the spectroscopic measurements of Kobulnicky, Kennicutt, & Pizagno 1999 who find $\text{H}\alpha/\text{H}\beta \sim 2.86$ which means there is little extinction. We suspect that there may have been an error in the calibration of the $\text{H}\beta$ image by Scowen 1992. $\text{H}\alpha$ fluxes listed by Fuentes-Masip, Castaneda, & Munoz-Tunon 2000 are consistent with those measured by Scowen 1992 so the $\text{H}\alpha$ fluxes measured by Scowen 1992 are sufficiently

well-calibrated. It is a concern that extinctions measured from the Balmer decrement might be biased by $H\beta$ absorption present in the stellar component (e.g., Dufour et al. 1980). However, after correcting for $H\beta$ absorption from the stellar component, Scowen 1992 found no strong changes in his correlation plots.

2.1. Comparing $H\alpha$ and $Pa\alpha$ Morphology

In Figures 1-3 we show the HST images for NGC 1512, NGC 2903, M 51 in both $Pa\alpha$ and $H\alpha$ lines. We found little correspondence between star clusters observed in the broad band images and the line emission maps. This makes it difficult to constrain the ages of the cluster based on $Pa\alpha$ equivalent widths. A number of star clusters were observed which were outside the region of line emission emission and so could correspond to regions where radiation pressure, ionization fronts, winds and supernovae have cleared the clusters of gas. In NGC 1512 and NGC 4449 the luminosities in $H\alpha$ of the faintest regions are $\sim 10^{37}$ ergs/s and so similar in luminosity to the Orion nebula (Kennicutt 1984) which contains one O star. Since H II regions cannot be much fainter than this, we suspect that there are no deeply embedded H II regions in these two galaxies. The faintest regions detected in NGC 2903 and M51 are an order of magnitude brighter and so could contain a few dozen O stars.

In NGC 1512, NGC 2903 and M51, there are few qualitative differences between the respective line emission images. In other words, almost all H II regions above the detection limit in $Pa\alpha$ were seen in both images. One region stands out as an exception to the above statement. This region in NGC 2903 is $0''.71$ east and $4''.17$ north of the nucleus (see Figure 1) and is significantly brighter in $Pa\alpha$ than in $H\alpha$. From the line ratio we estimate $A_V \sim 4$, however we did not see a peak in the $H\alpha$ line image; instead the line emission is diffuse and may not be emitted from the same spatial region. Previous studies have measured large extinctions in the nucleus of this galaxy ($A_V \sim 15$; Lebofsky & Rieke 1979) as well as high gas densities (Jackson et al. 1991) so this region may be an example of an obscured region.

Total $Pa\alpha$ and $H\alpha$ fluxes across our NGC 2903 images are 4.5×10^{-13} and 5.3×10^{-13} ergs $cm^{-2}s^{-1}$ respectively. We can compare these values to the $Br\alpha$ and $Br\gamma$ fluxes measured by Beck, Beckwith, & Gatley 1984 in an $8''$ diameter aperture. We would predict $Br\alpha$ and $Br\gamma$ fluxes of 1.53×10^{-13} , and 5.30×10^{-14} ergs $cm^{-2}s^{-1}$ respectively, using an A_V of 3.06 consistent with the $Pa\alpha$ and $H\alpha$ line ratio across this aperture. Our estimated $Br\alpha$ and $Br\gamma$ fluxes are consistent with those measured by Beck, Beckwith, & Gatley 1984, $1.4 \pm 0.18 \times 10^{-13}$ and $3.5 \pm 1.2 \times 10^{-14}$ respectively. The extinction we estimate $A_V \sim 3 - 4$ is therefore consistent with line fluxes and ratios measured by Beck, Beckwith, & Gatley 1984, but substantially lower than that, $A_V \sim 15$, measured from broad and narrow band imaging near the $10\mu m$ silicate absorption feature (Lebofsky & Rieke 1979). The region identified above is not bright enough (it is only 1/20th the total) in $Pa\alpha$ to dominate the total $Pa\alpha$ emission in the $8''$ nuclear region. Since the line ratios agree with $A_V \sim 3 - 4$, it is also unlikely that this region dominates the $Br\alpha$ emission.

The total $10\mu\text{m}$ flux roughly corresponds to that expected if a moderate fraction (e.g. 1/2) of the total bolometric luminosity in the UV (needed to account for the line emission) is re-radiated by dust (Beck, Beckwith, & Gately 1984). The $10\mu\text{m}$ emission is most likely to be emitted from the extended region we see in the line emission maps and not from a single deeply embedded region. The most likely explanation for the discrepancy between the extinctions we measure and that estimated at $10\mu\text{m}$ is that the $10\mu\text{m}$ spectrum contains structure from by PAH emission which caused Lebofsky & Rieke 1979 to overestimate the depth of the silicate absorption feature (see for example Siebenmorgen, Krügel, & Zota 1999). The extinction we estimate near the nucleus of NGC 6946 ($A_V \sim 4.6$) is also significantly lower than that estimated by Lebofsky & Rieke 1979 ($A_V \sim 50$).

3. A comparison between gas surface density, metallicity and extinction

For a distant galaxy we would like to derive star formation rates based on the emission line flux. We therefore desire a way to estimate the total emission in this line that would be emitted in the absence of extinction. In the comparison between $\text{H}\alpha$ and $\text{Pa}\alpha$ images we found no evidence for a population bright HII regions that are extremely red compared to the average. The scatter in A_V in each galaxy region (approximately ± 0.5) is less than the differences in the mean values which range from a mean $A_V \sim 3.3$ to 0. Because the mean values span a large range, we are prompted to look for correlations between this value and environmental properties.

To compare extinctions in different galactic environments we must first compile information from the literature on the metallicities and gas densities in the various regions of these galaxies. These are listed in Table 7 with references to the literature from which they were taken. The gas densities are primarily taken from single dish CO measurements with similar aperture sizes. When necessary we have corrected published values of CO so that we used the same conversion factor of $\text{N}(\text{H}_2) = 2.8 \times 10^{20} \text{ cm}^{-2} I_{\text{CO}} (\text{K km s}^{-1})$ (Scoville et al. 1987). The metallicities were primarily taken from Zaritsky et al. (1994). We estimate that the uncertainties in the gas density (approximately a factor of 2) and metallicity measurements (approximately 0.3 dex) are smaller than the variations between the measurements in different galaxies and galaxy regions.

We did not find a measured gas mass in NGC 1512 so we estimate the gas surface density based on the color map made from the broad band V ($0.5\mu\text{m}$) and H band ($1.6\mu\text{m}$) images. We observed a change in color of $\Delta(\text{V}-\text{H}) \sim 0.4$ between the circumnuclear ring and the region interior and exterior to it. We assume that the dust is a foreground screen for half of the light (for the bulge stars that are located behind the gas). This is equivalent to assuming that the scale length of the gas is smaller than that of the stars. This change in color then corresponds to $A_V \sim 1.3$ and a gas surface density in hydrogen of $\Sigma_H \sim 19 M_\odot \text{ pc}^{-2}$ (based on the A_V to $\text{N}(\text{H})$ conversion and extinction law of Mathis 1990).

We did not find any optical spectroscopy for NGC 1512 in the literature. However, we can use

the correlation between absolute magnitude and central metallicity found by Garnett et al. 1997 to estimate the metallicity in its circumnuclear ring. This galaxy has an absolute magnitude of $M_B \sim -18.9$ (assuming a distance of 9.5 Mpc from Tully 1988 with a Hubble constant of 75 $\text{km s}^{-1} \text{Mpc}^{-1}$). The galaxy has an inclination corrected circular velocity of $v_c \approx 173 \text{ km/s}$. From Figure 4 of Garnett et al. 1997 we estimate that NGC 1512 should have a central metallicity that is approximately solar.

To increase the size of our comparison sample we also compile the properties of H II regions as a function of radius in M101 and M51. H II region extinctions and luminosities in M101 were taken from Scowen et al. 1992 and are restricted to the 200 brightest H II regions. To describe the azimuthal gas density in M101 we summed the azimuthal molecular and atomic hydrogen gas mass densities reported by Kenney, Scoville & Wilson 1991. The metallicity gradient was taken from Kennicutt & Garnett 1996. H II region extinctions and luminosities in M51 were taken from Scowen 1992 and are restricted to be from the brightest H II regions defined as having an observed flux in $\text{H}\alpha$ greater than $10^{-14} \text{ erg cm}^{-2} \text{ s}^{-1}$. Molecular and atomic hydrogen gas densities in M51 were taken from Rydbeck, Hjalmarson & Rydbeck 1985 and Scoville & Young 1983. The oxygen abundance gradient in M51 were taken from Zaritsky, Kennicutt & Huchra 1994.

3.1. Weighting

We approach the problem of correcting for extinction by considering a sum over individual H II regions and by deriving a correction that can be multiplied by the total observed flux in the line to obtain the true one. This procedure is one way of averaging over a large scatter in extinctions and allows us to look for trends between the mean extinction and environmental properties. The correction we can describe as a luminosity weighted mean extinction. To derive this correction we sum over the corrected fluxes of each region, so it involves a luminosity weighted sum. This makes the estimate more robust than using the mean extinction computed from the distribution of extinctions measured towards each region. The mean computed from the distribution would be more dependent on the faintest HII regions and so noisier and less robust than the luminosity weighted mean extinctions computed as in equation (3) below.

We denote the flux in $\text{H}\alpha$ from a region i by $F_{H\alpha,i}$. We denote the sum of observed fluxes over a larger area as $F_{H\alpha} = \sum_i F_{H\alpha,i}$. We denote the true or corrected emission as

$$F_{H\alpha,corr} = \sum_i F_{H\alpha,i,corr}. \quad (1)$$

We aim to estimate a factor $a_{H\alpha}$ such that we can multiply the observed total flux in a large region to obtain the true or corrected emission.

$$F_{H\alpha,corr} = a_{H\alpha} F_{H\alpha}. \quad (2)$$

We correct the fluxes from each region using the extinctions derived from the line ratios and then sum the regions to estimate $F_{H\alpha,corr}$. At the same time we sum the uncorrected fluxes to get $F_{H\alpha}$.

From the ratio of $F_{H\alpha}$ and $F_{H\alpha,corr}$ we estimate the correction factor $a_{H\alpha}$ that we need to obtain the true or corrected emission from the observed total. This is converted to a mean extinction at the wavelength of $H\alpha$ by

$$\overline{A(H\alpha)} \equiv -2.5 \log a_{H\alpha}. \quad (3)$$

A similar mean extinction can also be calculated for $\text{Pa}\alpha$. This can be compared to the extinction estimated from the ratio of the total $\text{Pa}\alpha$ and $H\alpha$ fluxes which we refer to as $A_{total}(H\alpha)$.

We calculate the luminosity weighted mean extinction (defined above) by summing over the $\text{Pa}\alpha$ and $H\alpha$ fluxes listed in Tables 2-6 for the nuclear regions of NGC 1512, NGC 2903, NGC 4449, M51 and NGC 6946. These mean extinctions are listed in Table 7. We also perform these sums using $H\alpha$ and $H\beta$ fluxes as a function of radius in M101 and M51 based on the Balmer decrement. The radial width over which we summed the properties of H II regions was 1 kpc for M51 and 1.5 kpc for M101. For comparison to an additional low metallicity system we also derive a similar estimate for the LMC based on the Balmer decrement. $H\alpha$ and $H\beta$ fluxes for LMC H II regions were taken from Caplan & Deharveng 1985 and we correct for Galactic extinction using a value of $A_B = 0.324$ (Schlegel et al. 1998).

In Table 7 we can compare $\overline{A(H\alpha)}$ with $A_{total}(H\alpha)$. $\overline{A(H\alpha)}$ allows us to correct the total observed $H\alpha$ flux for reddening based on the reddenings to each H II region. We see a tendency for $\overline{A(H\alpha)}$ to be somewhat higher than that estimated from the line ratio of the integrated fluxes ($A_{total}(H\alpha)$). The differences are small because the dispersion in the extinctions between individual H II regions in each galaxy is low. A star formation rate estimated from the total $H\alpha$ line flux and corrected with an extinction based on the $H\alpha/\text{Pa}\alpha$ line ratio is likely to be quite accurate.

We plot our mean extinctions (defined in Eqn 3) versus gas density in Figure 4a. As expected there is a correlation between mean extinction and local gas density. However some of the correlation may be due to the dependence of the CO to H_2 conversion factor on metallicity. To take this dependence into account we correct the H_2 by a factor that depends on the metallicity and display the corrected gas density in Figure 4b. Our correction assumes an increase in the conversion factor by 4.6 when the oxygen abundance drops by a factor of 10 (Wilson 1995). Extending this relation towards metallicities larger than solar is reasonable since galaxies with metallicities greater than solar are expected to have lower conversion factors (e.g., Nakai & Kuno 1995). The correlation between gas density and mean extinction is not significantly changed.

It is difficult to separate between the role of gas density and that of metallicity since the densest regions also correspond to the most metal rich. However as we see in Figure 4c, metallicity alone is not sufficient to account for the large variation in our mean extinctions.

The dust density is the quantity most likely to affect the reddening so we desire a comparison between our extinction values and the dust surface density. We can estimate the dust surface density from the gas density using a metallicity dependent gas to dust mass ratio. The gas to dust ratio may correlate better with the carbon abundance than with the oxygen abundance

(Bohlin, Savage, & Drake 1978; Martin, Maurice, & Lequeux 1989). To convert between oxygen abundance and carbon abundance we use the relation measured by Garnett et al. 1995 [$\log(C/O) \approx 0.54 \log(O/H) + 1.6$]. We assume that at solar metallicity the gas to dust mass ratio is 120. To estimate the dust surface density we multiply the solar dust to gas ratio by the gas density and the ratio between the carbon abundance predicted from the oxygen abundance and that at solar. The relation between mean extinction and estimated dust density is shown in Figure 4d. The dashed line plotted in Figure 4d corresponds to that predicted for a uniform medium with the H II regions located in the middle of the dust distribution. We find that the correlations we have seen between mean extinction, gas density and metallicity are consistent with an approximately linear relation between the log of the dust density and mean extinction.

For the high dust densities, the mean extinctions expected are somewhat higher than those observed. In Figure 4d we plotted the extinction predicted if the H II regions were in the mid plane of a uniform disk. These deviations would be predicted from a model which takes into account the patchiness of the ISM (e.g., Calzetti et al. 1996). To illustrate this we have also plotted in Figure 4d a patchy dust model for a two component dust model with an extinction ratio of four and an area filling factor of 0.5. However such a model would result in a larger scatter (greater than ± 0.75) in the extinctions towards individual regions than we measured. A more realistic patchy dust model may match the extinction and mean gas density. There could be nearby dense molecular clouds lacking H II regions which would have contributed to the mean gas density in the region but not to the H II region extinctions.

4. Summary and Discussion

In this paper we have presented a comparative study between $\text{Pa}\alpha$ and $\text{H}\alpha$ in the central regions of five galaxies. For three galaxies we have HST images in both lines and the morphologies of the respective line emission maps are remarkably similar. The dispersion in extinctions is about a magnitude for the H II regions in each galaxy and is smaller than the differences between the mean extinctions. We find no evidence for a population of bright heavily embedded H II regions.

Only one bright region, in NGC 2903, was detected clearly in the $\text{Pa}\alpha$ image and was faint or not seen in the $\text{H}\alpha$ image. However this region does not dominate the $\text{Pa}\alpha$ flux of the nuclear star forming region and is also unlikely to dominate the $\text{Br}\alpha$ emission. This suggests that an estimate of the star formation rate based on a mean extinction and either the $\text{H}\alpha$ or $\text{Pa}\alpha$ flux is likely to be fairly accurate. We suspect that some previous studies of the silicate absorption feature at $10\mu\text{m}$ may have overestimated the extinction towards the nuclei of NGC 2903 and NGC 6946 because of contamination by PAH features.

We have compared mean extinctions as a function of gas density and metallicity and find correlations between these quantities. The correlations between mean extinction, gas density and metallicity are consistent with an approximately linear relation between the log of the dust

density and mean extinction. This trend is expected if the H II regions tend to be located near the mid-plane of a gas disk and emerge from their parent molecular clouds soon after birth. Radiation pressure and ionization fronts are expected to clear a young star forming region of dense gas on a timescale of 10^5 years (Ferland 1998) whereas H II regions should exist for a few times 10^6 years. It would be unlikely to detect an H II region in a region with extinction significantly higher than the mean predicted from the local gas density. This may provide a partial explanation for the low dispersion in extinctions that we measured in each galaxy.

We expect that forthcoming high resolution CO and HI surveys will allow a more careful comparison between the statistical properties of H II regions and the gas distribution. It may be possible to study correlations between the patchy distribution of the ISM, the tendency for star forming regions to evacuate themselves of dense gas, and large scale gaseous structures cause by bars and spiral arms. The relationships presented here may allow more accurate estimates of star formation rates in galaxy regions which contain gas densities up to a few hundred $M_\odot \text{ pc}^{-2}$. Above this level it is likely that a significant fraction of the line emission is absorbed even in the near-infrared and mid or far infrared measurements would be required (e.g., Kennicutt 1998). Further work on the trends discussed here may make it possible to more accurately measure star formation rates and constrain gas densities in distant galaxies.

Support for this work was provided by NASA through grant number GO-07869.01-96A from the Space Telescope Institute, which is operated by the Association of Universities for Research in Astronomy, Incorporated, under NASA contract NAS5-26555. We also acknowledge support from NASA project NAG-53359 and NAG-53042 and from JPL Contract No. 961633. This work could not have been done without the help of Don Garnett. We also thank Rob Kennicutt, Marcia Rieke, George Rieke, Torsten Böker, Chad Engelbracht and Karl Gordon for helpful discussions. We thank Gil Rivlis for helping us scan and convert tables. We thank Rob Kennicutt for providing us with the $\text{H}\alpha$ image of NGC 6946. This research has made use of the NASA/IPAC Extragalactic Database (NED) which is operated by the Jet Propulsion Laboratory, California Institute of Technology, under contract with the National Aeronautics and Space Administration. We thank the referee for comments which have improved this paper.

REFERENCES

Beck, S. C., Beckwith, S., & Gatley, I. 1984, *ApJ*, 279, 563

Bohlin, R. C., Savage, B. D., & Drake, J. F. 1978, *ApJ*, 224, 132

Böker, T. et al. 1999, *ApJS*, 124, 95

Bresolin, F., Kennicutt, R. C., Jr., & Garnett, D. R. 1999, *ApJ*, 510, 104

Calzetti, D., Kinney, A. L., & Storchi-Bergmann, T. 1996, *ApJ*, 458, 132

Caplan, J., & Deharveng, L. 1985, *A&AS*, 62, 63

Cohen, R. S., Dame, T. M., Garay, G., Montani, J., Rubio, M., & Thaddeus, P. 1988, *ApJ*, 331, L95

Dufour, R. J., Talbot, R. J., Jr., Jensen, E. B., & Sheilds G. A. 1980, *ApJ*, 236, 119

Fuentes-Masip, O., Castaneda, H. O., & Munoz-Tunon, C. *ApJ*, 119, 2166

Ferland, G. J. 1998, (astro-ph/9808107)

Garnett, D. R., Shields, G. A., Skillman, E. D., Sagan, S. P., & Dufour, R. J. 1997, *ApJ*, 489, 63

Garnett, D. R., Skillman, E. D., Dufour, R. J., Peimbert, M., Torres-Peimbert, S., Terlevich, R., Terlevich, E., & Shields, G. A. 1995, *ApJ*, 443, 64

Heckman, T. M., Robert, C., Leitherer, C., Garnett, D. R., & van der Rydt, F. 1998, *ApJ*, 503, 646

Hunter, D. A., & Thronson, H. A., Jr. 1996, *ApJ*, 461, 202

Jackson, J. M., Eckart, A., Cameron, M., Wild, W., Ho, P. T. P., Pogge, R. W., & Harris, A. I. 1991, *ApJ*, 375, 105

Heydari-Mayaleri, M., & Testor, G. 1985, *A&A*, 144, 98

Hyman, S. D., Lagacey, C. K., Weiler, K. W. & Van Dyk, S. D. 2000, *AJ*, 119, 1711

Kenney, J. D. P., Scoville, N. Z., & Wilson, C. D. 1991, *ApJ*, 366, 432

Kennicutt, R. C., Jr. 1998, *ApJ*, 498, 541

Kennicutt, R. C., Jr. 1983, *ApJ*, 272, 54

Kennicutt, R. C., Jr. 1984, *ApJ*, 287, 116

Kennicutt, R. C., Jr., & Garnett, D. R. 1996, *ApJ*, 456, 504

Kennicutt, R. C., Jr., Keel, B. C., & Blaha, C. A. 1989, AJ, 97, 1022

Kobulnicky, H. A., Kennicutt, R. C., Jr., & Pizagno, J. L. 1999, ApJ, 514, 544

Kuno, N., & Nakai, N. 1997, PASJ, 49, 279

Lebofsky, M. J., & Rieke, G. H. 1979, ApJ, 229, 111

Luks, Th., & Rohlfs, K. 1992, A&A, 263, 41

Marconi, A., Oliva, E., van der Werf, P. P., Maiolino, R., Schreier, E. J., Macchetto, F., & Moorwood, A. F. M. 2000, A&A, 357, 24

Martin, P., & Friedli, D. 1999, A&A, 346, 769

Martin, N., Maurice, E., & Lequeux, J. 1989, A&A, 215, 219

Mathis, J. S. 1990, ARAA, 28, 37

McCall, M. L., Rybski, P. M., & Shields, G. A. 1985, ApJS, 57, 1

McLeod, B. 1997, proceedings of the 1997 HST Calibration Workshop, eds. S. Casertano, R. Jedrzejewski, T. Keyes, and M. Stevens, published by the Space Telescope Science Institute, Baltimore, MD, p. 281

Nakai, N., & Kuno, N. 1995, PASJ, 47, 761

Osterbrock, D.E. 1989, *Astrophysics of Gaseous Nebulae and Active Galactic Nuclei*, University Science Books, Mill Valley, CA

Rydbeck, G., Hjalmarson, A., & Rydbeck, O. E. H. 1985, A&A, 144, 282

Sandage, A. & Tammann, G. A. 1975, ApJ, 196, 313

Schmidt, M. 1959, ApJ, 129, 243

Scoville, N., & Young J. S. 1983, ApJ, 265, 148

Scoville, N. Z., Yun, M. S., Sanders, D. B., Clemens, D. P., & Waller, W. H. 1987, ApJS, 63, 821

Scowen, P. A., Dufour, R. J., & Hester J. J. 1992, AJ, 104, 92

Scowen, P. A. 1992, PhD thesis, Rice University

Schlegel, D., Finkbeiner, D. P., & Davis, M. 1998, ApJ, 500, 525

Siebenmorgen, R., Krügel, E., & Zota, V. 1999, A&A, 351, 140

Stewart, S. G. el al. 2000. ApJ, 521, 201

Storchi-Bergmann, T., Calzetti, D., & Kinney, A. L. 1994, *ApJ*, 429, 572

Tully, R. B. 1988, *Nearby Galaxies Catalog*, Cambridge University Press, Cambridge

Wilson, C. D. 1995, *ApJ*, 448, L97

Young, J. S., & Scoville, N. Z. 1982, *ApJ*, 258, 467

Young, J. S., et al. 1995, *ApJS*, 98, 219

Zaritsky, D., Kennicutt, R. C., Jr., & Huchra, J. P. 1994, *ApJ*, 420, 87

Fig. 1.— HST images of the circumnuclear ring of NGC 2903. The H α image was constructed from WFPC2 images. The Pa α was observed with NICMOS Camera 3 and constructed from F187N and F160W images. The V-H color map was constructed from the F555W and F160W images. Colors from V-H = 2.0 (white) to 3.5 (black) are shown. Axes are given in arcsec from the nucleus. There is a bright source at 0''.71 east, and 4''.17 north from the nucleus evident in the Pa α image but not the H α image.

Fig. 2.— HST images of the circumnuclear ring of NGC 1512. The H α image was constructed from WFPC2 images. The Pa α was observed with NICMOS Camera 2 and constructed from F187N and F160W images. The V-H color map was constructed from the F547M and F160W images. Colors range from V-H = 2.5 (white) to 3.3 (black) are shown. Axes are given in arcsec from the nucleus. We found no evidence for bright embedded H II regions.

Fig. 3.— HST images of a region about $20''$ to the north and $20''$ to the east of the nucleus in M51. The $\text{H}\alpha$ image was constructed from WFPC2 images. The $\text{Pa}\alpha$ was observed with NICMOS Camera 3 and constructed from F187N and F190N images. The V-H color map was constructed from the F547M and F160W images. Colors from $\text{V-H} = 2.5$ (white) to 3.3 (black) are shown. Axes are given in arcsec from the brightest region listed in Table 6. See Table 6 for the coordinates of this region.

Fig. 4.— a) The relation between the luminosity weighted extinction and the azimuthal hydrogen gas density. NGC 1512, NGC 2903, NGC 4449, NGC6946, the LMC, and the north east position of M51 are plotted by name. The M101 and M51 azimuthal averages are plotted as solid triangles and open squares, respectively, where each point represents an average at a different radius. The dashed line shows the linear relation between A_V and half of the gas column depth (assuming the relation between hydrogen column depth and extinction from Mathis 1990). We use half of the gas column, assuming that the H II regions are embedded in the gas disk. The gas densities have been estimated with a CO conversion factor of $N(H_2) = 2.8 \times 10^{20} \text{ cm}^{-2} I_{CO}$ (K km s^{-1}) (Scoville et al. 1987). b) Similar to a) however we have corrected the hydrogen gas densities by using a CO conversion factor that depends on metallicity (see text for details). c) Dependence of the luminosity weighted extinction with metallicity only. We see this correlation in part because the regions with higher gas density also correspond to regions of higher metallicity. The dotted line shows the extinction predicted from a gas surface density of $10 M_\odot \text{ pc}^{-2}$ and a dust to gas fraction that depends on the carbon abundance. The metallicity alone is not sufficient to account for the variations in extinctions. d) Dependence of the luminosity weighted extinction (defined in Eqn 3) with estimated dust surface density. The dust surface density was estimated from the corrected gas densities (shown in b) by scaling with the carbon abundance (see text for details). The dashed line shows the linear relation between A_V and half of the dust column depth. The dot dashed line is a 2 component patchy dust model with an area filling factor of 50% and an opacity ratio of 4. This model illustrates that a patchy medium would have a lower mean extinction than that predicted directly from the dust density.

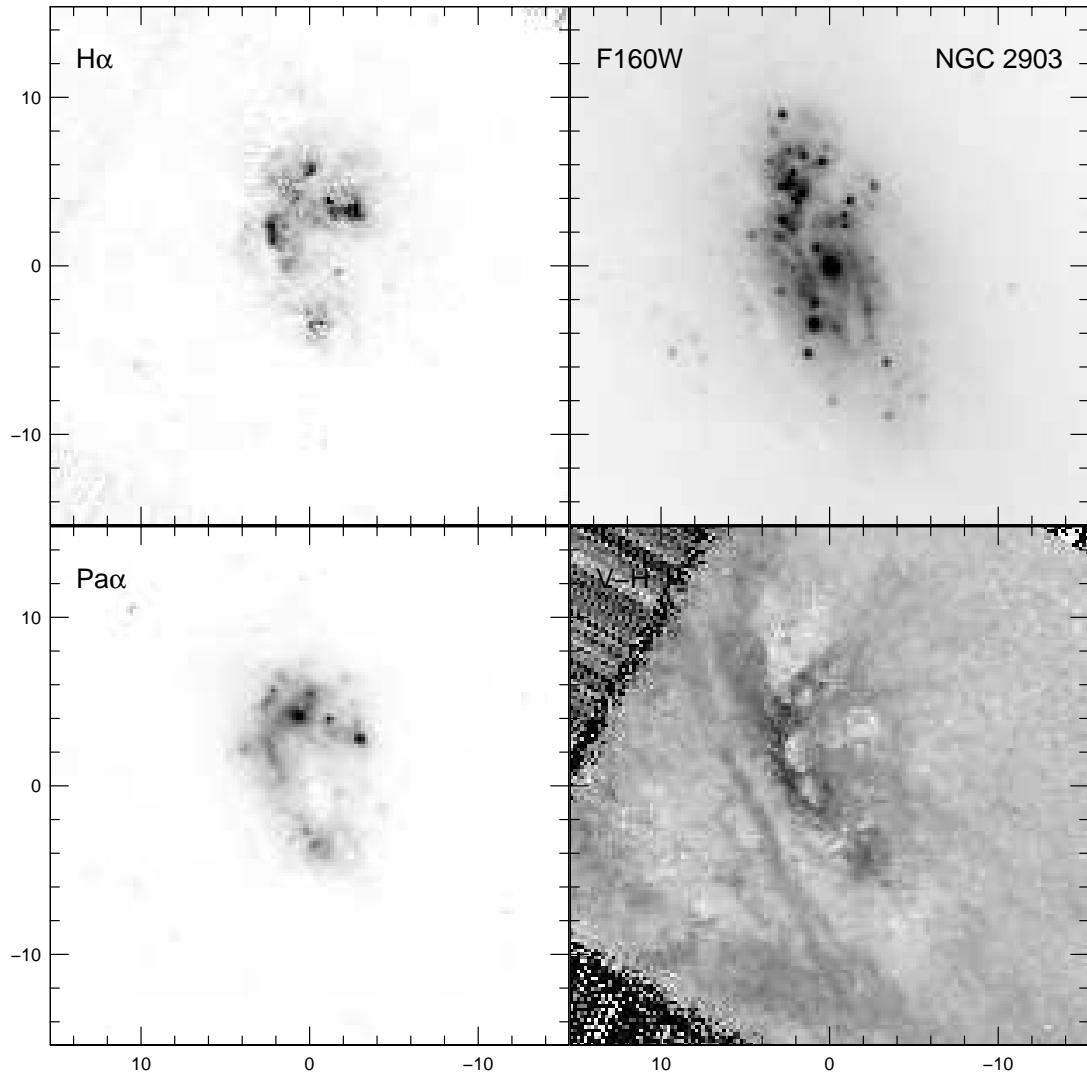


Fig. 1.— HST images of the circumnuclear ring of NGC 2903. The $\text{H}\alpha$ image was constructed from WFPC2 images. The $\text{Pa}\alpha$ was observed with NICMOS Camera 3 and constructed from F187N and F160W images. The V-H color map was constructed from the F555W and F160W images. Colors from $\text{V-H} = 2.0$ (white) to 3.5 (black) are shown. Axes are given in arcsec from the nucleus. There is a bright source at $0.^{\circ}71$ east, and $4.^{\circ}17$ north from the nucleus evident in the $\text{Pa}\alpha$ image but not the $\text{H}\alpha$ image.

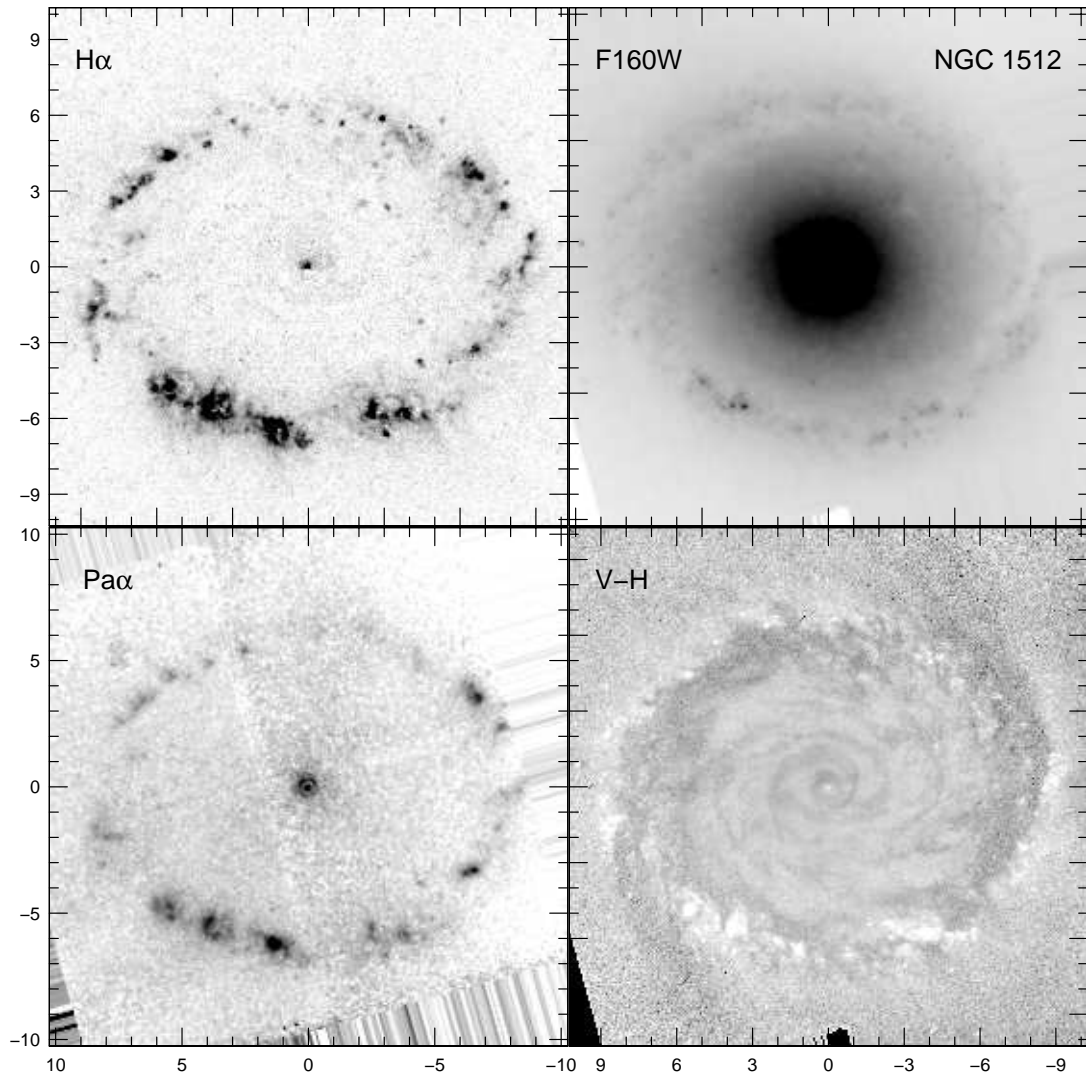


Fig. 2.— HST images of the circumnuclear ring of NGC 1512. The $\text{H}\alpha$ image was constructed from WFPC2 images. The $\text{Pa}\alpha$ was observed with NICMOS Camera 2 and constructed from F187N and F160W images. The V-H color map was constructed from the F547M and F160W images. Colors from V-H = 2.5 (white) to 3.3 (black) are shown. Axes are given in arcsec from the nucleus. We found no evidence for bright embedded HII regions.

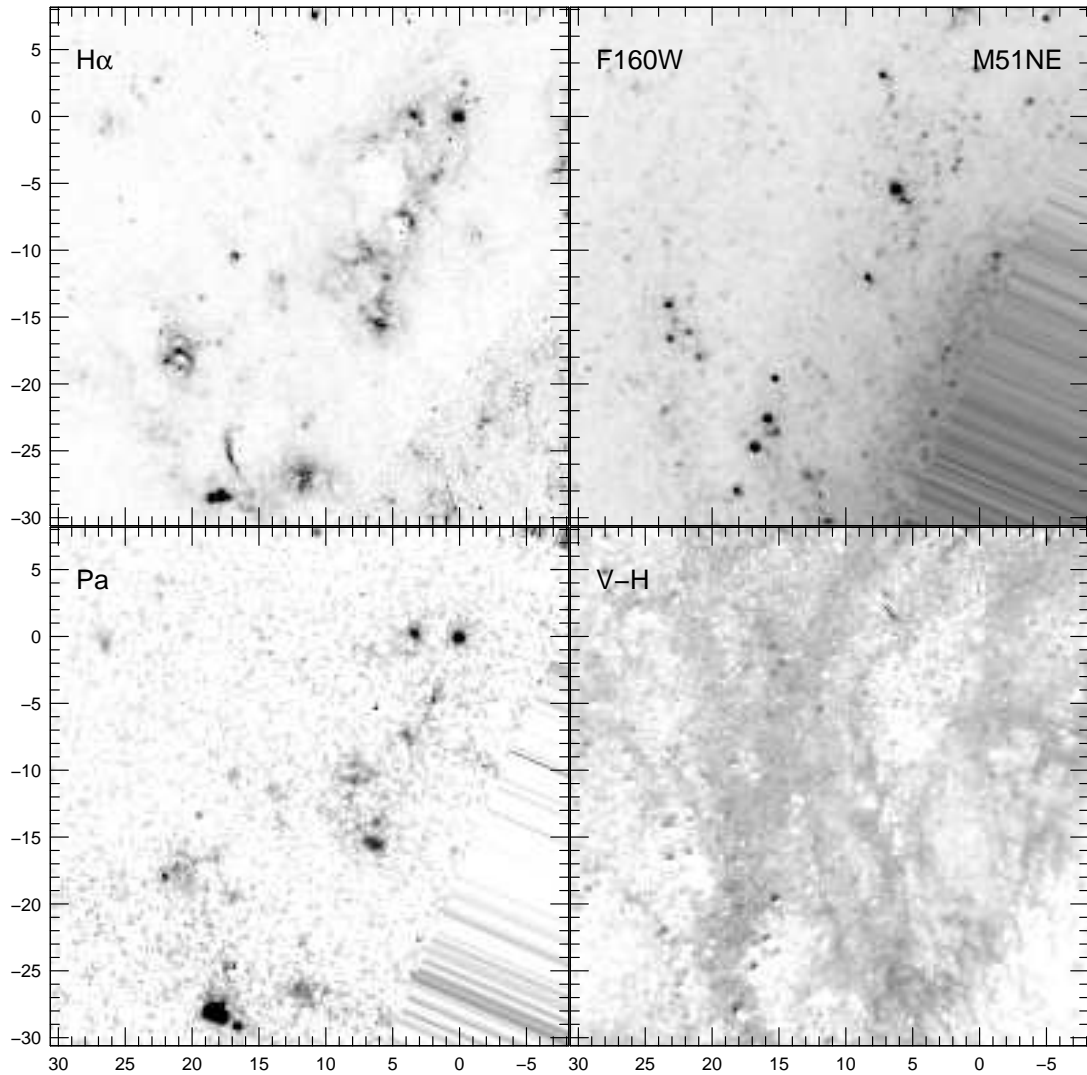


Fig. 3.— HST images of a region about $20''$ to the north and $20''$ to the east of the nucleus in M51. The $\text{H}\alpha$ image was constructed from WFPC2 images. The $\text{Pa}\alpha$ was observed with NICMOS Camera 3 and constructed from F187N and F190N images. The V-H color map was constructed from the F547M and F160W images. Colors from $\text{V-H} = 2.5$ (white) to 3.3 (black) are shown. Axes are given in arcsec from the brightest region listed in Table 6. See Table 6 for the coordinates of this region.

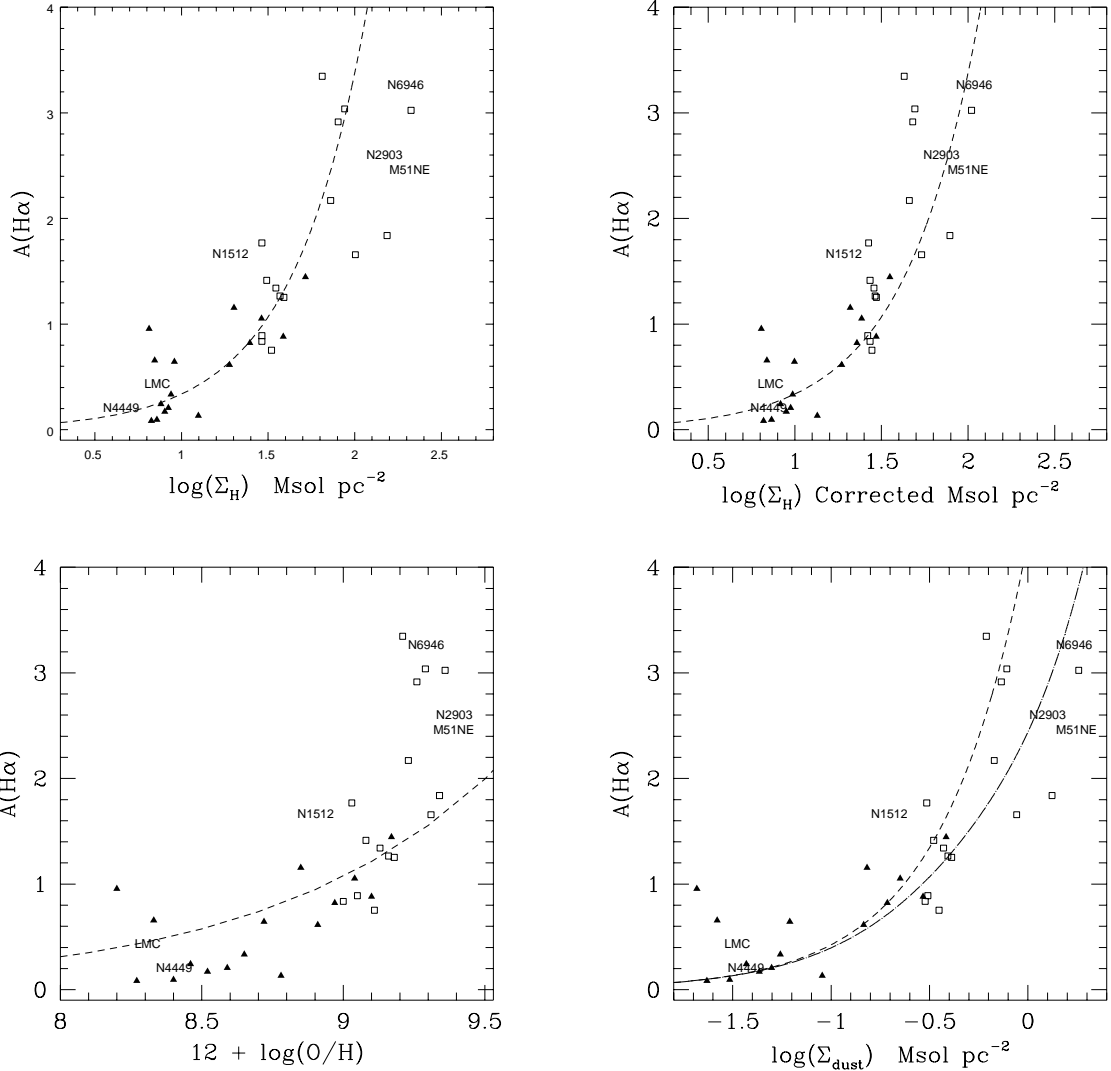


Fig. 4.— a) The relation between the luminosity weighted extinction and the azimuthal hydrogen gas density. NGC 1512, NGC 2903, NGC 4449, NGC6946, the LMC, and the north east position of M51 are plotted by name. The M101 and M51 azimuthal averages are plotted as solid triangles and open squares, respectively, where each point represents an average at a different radius. The dashed line shows the linear relation between A_V and half of the gas column depth (assuming the relation between hydrogen column depth and extinction from Mathis 1990). We use half of the gas column, assuming that the HII regions are embedded in the gas disk. The gas densities have been estimated with a CO conversion factor of $N(H_2) = 2.8 \times 10^{20} \text{ cm}^{-2} I_{CO}$ (K km s^{-1}) (Scoville et al. 1987). b) Similar to a) however we have corrected the hydrogen gas densities by using a CO conversion factor that depends on metallicity (see text for details). c) Dependence of the luminosity weighted extinction with metallicity only. We see this correlation in part because the regions with higher gas density also correspond to regions of higher metallicity. The dotted line shows the extinction predicted from a gas surface density of $10 M_\odot \text{ pc}^{-2}$ and a dust to gas fraction that depends on the carbon abundance. The metallicity alone is not sufficient to account for the variations in extinctions. d) Dependence of the luminosity weighted extinction (defined in Eqn 3) with estimated dust surface density. The dust surface density was estimated from the corrected gas densities (shown in b) by scaling with the carbon abundance (see text for details). The dashed line shows the linear relation between A_V and half of the dust column depth. The dot dashed line is a 2 component patchy dust model with an area filling factor of 50% and an opacity ratio of 4. This model illustrates that a patchy medium would have a lower mean extinction than that predicted directly from the dust density.

Table 1. HST archival images

galaxy	Pa α	continuum	H α	continuum
NGC 1512	F187N/NIC2	F160W/NIC2	F658N	F547M
NGC 2903	F187N/NIC3	F160W/NIC3	F656N	F555W
M51	F187N/NIC3	F190N/NIC3	F656N	F547M
NGC 4449	F187N/NIC3	F160W/NIC3		
NGC 6946	F187N/NIC3	F190N/NIC3		

Note. — Line and continuum filters on HST used to make the Pa α and H α line emission maps shown in Figures 1-3 and used to measure H II region intensities and line ratios listed in Tables 2-6. The near-infrared images were observed with NICMOS and the filter names are followed by the NICMOS camera used for the observation. The pixel size for the NICMOS camera 2 (NIC2) is $\sim 0''.076$, and for the NICMOS camera 3 (NIC3) is $\sim 0''.204$.

Table 2. H II regions in NGC 1512

Δ RA "	Δ DEC "	Flux $H\alpha$ 10^{-14} ergs cm^{-2} s^{-1}	$F_{Pa\alpha}/F_{H\alpha}$	A_V	$L_{H\alpha}$ 10^{37} ergs s^{-1}
(1)	(2)	(3)	(4)	(5)	(6)
1.29	-6.16	36.97	0.32	1.62	13.60
3.65	-5.79	10.83	0.40	1.98	5.22
3.88	-5.24	18.68	0.31	1.54	6.44
5.42	-5.09	10.21	0.41	2.01	5.02
5.42	-4.67	14.85	0.30	1.49	4.92
5.93	-4.71	6.67	0.52	2.42	4.46
7.51	-1.92	2.61	0.79	3.07	2.86
8.28	-1.54	5.41	0.36	1.82	2.31
7.30	2.58	4.39	0.33	1.66	1.66
6.76	3.22	5.35	0.39	1.92	2.46
5.40	4.51	12.24	0.17	0.57	2.03
4.72	4.41	1.75	0.55	2.51	1.25
3.81	4.94	3.41	0.43	2.09	1.78
2.48	5.40	2.53	0.90	3.28	3.27
-6.47	3.95	5.92	0.52	2.41	3.93
-6.76	3.57	8.11	0.63	2.70	6.75
-7.52	-1.59	1.46	0.88	3.25	1.84
-6.61	-3.26	6.48	0.75	2.99	6.70
-6.58	-3.27	6.27	0.79	3.07	6.89

Note. — We did aperture photometry in $0''.75$ radius apertures. Offsets are given with respect to the position of the nucleus; RA(2000) = 4:03:54.131, DEC(2000)= -43:20:56.54, as measured from the HST pointing. Columns: (1) Offset in RA from the nucleus. A positive offset is east of the nucleus; (2) Offsets in DEC from the nucleus. A positive offset is north of the nucleus; (3) Measured flux in $H\alpha$. Uncertainty in the sky value causes an error of $\sim \pm 5\%$ in the faintest regions; (4) Ratio of flux in $Pa\alpha$ to $H\alpha$. Uncertainty in the sky value causes an error of $\sim \pm 13\%$ in the measurement of the $Pa\alpha$ flux in the faintest regions; (5) A_V computed from the ratio. The distribution of extinctions is centered at $A_V = 1.8$ with a standard deviation of 0.7; (6) Luminosity in $H\alpha$ which has been corrected for extinction using A_V given in column (5). We assume a distance of 9.5 Mpc (Tully 1988; $H_0 = 75$ km s^{-1} Mpc $^{-1}$).

Table 3. H II regions in NGC 2903

Δ RA "	Δ DEC "	Flux H α 10^{-14} ergs cm $^{-2}$ s $^{-1}$	$F_{Pa\alpha}/F_{H\alpha}$	A_V	$L_{H\alpha}$ 10^{38} ergs s $^{-1}$
(1)	(2)	(3)	(4)	(5)	(6)
-2.95	2.79	1.79	0.91	3.21	9.56
-1.38	3.19	2.00	0.47	2.13	4.73
-1.11	4.02	2.50	0.47	2.12	5.87
-0.03	5.45	1.63	0.89	3.17	8.46
0.71	4.17	1.44	1.66	4.18	15.99
2.17	5.61	0.70	1.47	3.98	6.70
2.58	5.04	0.80	1.35	3.84	6.85
3.81	2.20	0.48	1.65	4.17	5.35
2.17	2.99	1.49	0.75	2.89	6.25
1.97	1.42	1.89	0.56	2.41	5.51
0.24	-2.66	0.75	1.04	3.42	4.71
-0.49	-3.36	1.23	0.81	3.02	5.68
-0.98	-3.98	0.55	1.48	4.00	5.29

Note. — We did aperture photometry in 0''.469 radius apertures. Offsets are given with respect to the position of the nucleus; RA(2000) = 9:32:09.98, DEC(2000)= +21:30:0.8, as measured from the HST pointing. Columns: (1) Offset in RA from the nucleus. A positive offset is east of the nucleus; (2) Offset in DEC from the nucleus. A positive offset is north of the nucleus; (3) Measured flux in H α . Uncertainty in the sky value causes an error of $\sim \pm 2\%$ in the faintest regions; (4) Ratio of flux in Pa α to H α . Uncertainty in the sky value causes an error of $\sim \pm 4\%$ in the measurement of the Pa α flux in the faintest regions; (5) A_V computed from the ratio. The distribution of extinctions is centered at $A_V = 3.3$ with a standard deviation of 0.7; (6) Luminosity in H α which has been corrected for extinction using A_V given in column (5). We assume a distance of 6.3 Mpc (Tully 1988; $H_0 = 75$ km s $^{-1}$ Mpc $^{-1}$).

Table 4. H II regions in NGC 4449

RA(2000) '' (1)	DEC(2000) '' (2)	Flux $\text{Pa}\alpha$ $10^{-14} \text{ ergs cm}^{-2} \text{ s}^{-1}$ (3)	$F_{\text{Pa}\alpha}/F_{\text{H}\alpha}$ (4)	A_V (5)	$L_{\text{H}\alpha}$ $10^{37} \text{ ergs s}^{-1}$ (6)
12:28:12.08	44:05:51.56	1.49	0.05	0.00	3.39
12:28:11.70	44:05:55.98	0.82	0.02	0.00	3.67
12:28:11.33	44:05:42.12	1.40	0.02	0.00	7.64
12:28:11.83	44:05:46.18	2.35	0.07	0.00	3.88
12:28:12.93	44:05:31.61	2.02	0.11	0.00	1.98
12:28:13.68	44:05:42.98	1.18	0.07	0.00	1.98
12:28:13.11	44:05:41.44	5.28	0.29	1.43	6.04
12:28:12.45	44:05:45.13	1.50	0.05	0.00	3.09
12:28:13.74	44:06:10.35	2.18	0.12	0.07	2.06
12:28:12.63	44:05:21.34	1.75	0.10	0.00	2.01
12:28:13.70	44:05:26.55	0.82	0.13	0.16	0.79
12:28:11.37	44:05:36.89	12.79	0.19	0.73	13.27

Note. — We did aperture photometry in $4''$ radius apertures to match the apertures used by Scowen (1992) to measure $\text{H}\alpha$ fluxes. Columns: (1) RA of emission peak in RA as we measure in the $\text{Pa}\alpha$ image; (2) DEC of emission peak as measured in the $\text{Pa}\alpha$ image; (3) Measured flux in $\text{Pa}\alpha$. Uncertainty in the sky value causes an error of $\sim \pm 11\%$ in the measurement of the $\text{Pa}\alpha$ flux in the faintest regions; (4) Ratio computed by using our $\text{Pa}\alpha$ flux and the $\text{H}\alpha$ flux measured by Scowen (1992) in the same region; (5) A_V computed from the ratio; (6) Luminosity in $\text{H}\alpha$ which has been corrected for extinction using given A_V given in column (5). We assume a distance of 3.05 Mpc (Stewart et al. 2000).

Table 5. H II regions in NGC 6946

Δ RA "	Δ DEC "	Flux $\text{Pa}\alpha$ $10^{-14} \text{ ergs cm}^{-2} \text{ s}^{-1}$	$F_{\text{Pa}\alpha}/F_{\text{H}\alpha}$	A_V	$L_{\text{H}\alpha}$ $10^{38} \text{ ergs s}^{-1}$
(1)	(2)	(3)	(4)	(5)	(6)
0.75	-1.49	28.20	2.03	4.60	163.16
-1.24	-15.97	1.28	0.47	2.24	5.34
-13.48	-10.16	1.74	0.86	3.21	8.30
-9.00	-23.62	3.50	0.82	3.15	16.57
-11.60	2.28	2.65	0.85	3.20	12.64
16.36	-22.69	1.29	0.55	2.48	5.55

Note. — We did aperture photometry in $2''.7$ radius apertures. Offset are given with respect to the position of the nucleus; RA(2000) = 20:34:52.33, DEC(2000) = +60:09:14.21, as measured from the HST pointing. Columns: (1) Offset in RA from the nucleus. A positive offset is east of the nucleus; (2) Offset in DEC for the nucleus. A positive offset is north of the nucleus; (3) Measured flux in $\text{Pa}\alpha$. Uncertainty in the sky value causes an error of $\sim \pm 11\%$ in the measurement of the $\text{Pa}\alpha$ flux in the faintest region; (4) Ratio of flux in $\text{Pa}\alpha$ to $\text{H}\alpha$. Uncertainty in the sky value causes an error of $\sim \pm 15\%$ in the measurement of the $\text{H}\alpha$ flux in the faintest region; (5) A_V computed from the ratio. The distribution of extinctions is centered at $A_V = 2.8$ with a standard deviation of 1.2; (6) Luminosity in $\text{H}\alpha$ which has been corrected for extinction using A_V given in column (5). We assume a distance of 5.5 Mpc (Tully 1988; $H_0 = 75 \text{ km s}^{-1} \text{ Mpc}^{-1}$).

Table 6. H II regions in M51

Δ RA "	Δ DEC "	Flux $H\alpha$ 10^{-15} ergs cm^{-2} s^{-1}	$F_{Pa\alpha}/F_{H\alpha}$	A_V	$L_{H\alpha}$ 10^{38} ergs s^{-1}
(1)	(2)	(3)	(4)	(5)	(6)
0.00	0.00	12.85	0.30	1.51	5.23
3.29	0.39	4.99	0.51	2.38	3.88
1.84	-4.58	3.01	0.42	2.05	1.83
3.86	-7.24	3.29	0.41	2.02	1.95
7.81	-10.60	2.11	0.65	2.77	2.20
6.12	-13.77	2.45	0.54	2.45	2.02
6.24	-15.54	3.99	0.58	2.59	3.62
12.04	-26.23	3.27	0.45	2.18	2.19
18.15	-27.76	3.89	2.61	5.01	21.97
16.51	-29.02	1.37	2.40	4.88	6.95

Note. — We did aperture photometry in $0''.41$ radius apertures. Offsets are given with respect to the first listed position; RA(2000) = 13:29:54.00, DEC(2000) = 47:12:11.86. Columns : (1) Offset in RA from the first listed position. A positive offset is east of the first position; (2) Offset in DEC from the first position. A positive offset is north of the first detected position nucleus; (3) Measured flux in $H\alpha$. Uncertainty in the sky value causes an error of $\sim \pm 4\%$ in the measurement of the $H\alpha$ flux in the faintest region; (4) Ratio of flux in $Pa\alpha$ to $H\alpha$. Uncertainty in the sky value causes an error of $\sim \pm 8\%$ in the measurement of the $H\alpha$ flux in the faintest region; (5) A_V computed from the ratio; (6) Luminosity in $H\alpha$ which has been corrected for extinction using A_V given in column (5). The assumed distance is 9.6 Mpc (Sandage & Tammann 1975).

Table 7. Integrated properties of H II regions, local gas density and metalicity

Galaxy	$\overline{A(H\alpha)}$	$\overline{A(Pa\alpha)}$	$A_{total}(H\alpha)$	12 + log(O/H)	M_{HI} $M_\odot \text{ pc}^{-2}$	M_{H2} $M_\odot \text{ pc}^{-2}$
(1)	(2)	(3)	(4)	(5)	(6)	(7)
NGC 1512	1.68	0.32	1.67	9.4		19
NGC 2903	2.62	0.48	2.67	8.9		147
NGC 4449	0.25	0.07	0.00	8.4	2.2	2.2
NGC 6946	3.28	0.61	3.26	9.3		195
M51NE	2.48	0.52	2.37	9.4		200
LMC	0.45			8.8	7	

Note. — Values for the mean extinctions $\overline{A(H\alpha)}$ and $\overline{A(Pa\alpha)}$ (defined in Equation 3) were derived from the $Pa\alpha$ fluxes and $Pa\alpha/H\alpha$ flux ratios listed in Tables 2-6 for all galaxies except the LMC. This can be compared to the extinction estimated from the ratio of the total $Pa\alpha$ and $H\alpha$ fluxes which we refer to as $A_{total}(H\alpha)$. The value for $\overline{A(H\alpha)}$ for the LMC was estimated from the fluxes and Balmer decrements listed by Caplan & Deharveng (1985). Metalicities are estimated for the region covered by our images. For NGC 1512 the central metalicity was estimated based on its luminosity and a gas density corresponding to the extinction we observe in our color map (see text). Central metalicities for NGC 2903, M51, and NGC 6494 were estimated from gradients and values listed by Zaritsky et al. (1994). The metalicity of NGC 4449 is that measured by Heckman et al. (1988). The gas density for the nucleus of NGC 2903 was estimated from the inclination corrected value by Jackson et al. (1991). The gas density for NGC 6946 is that listed by Young et al (1995) and is averaged over the NICMOS Camera 3 field of view ($\sim 45''$). The gas densities for NGC 4449 are estimated using an average of values listed in Hunter & Thronson (1996). Gas densities for the LMC were taken from Luks & Rohlfs (1992) and Cohen et al. (1988). The molecular gas density for the NE position of M51 was taken from Kuno & Nakai (1997). When necessary we have corrected published values so that we used the same conversion factor of $N(H_2) = 2.8 \times 10^{20} \text{ cm}^{-2} I_{CO}$ (K km s^{-1}) (Scoville et al. 1987).